Journal of Computational Physics 231 (2012) 6086–6096

Contents lists available at SciVerse ScienceDirect

Journal of Computational Physics

journal homepage: www.elsevier.com/locate/jcp

Boundary conditions for hemodynamics: The structured tree revisited

W. Cousins [a,1], P.A. Gremaud [a,b,*,2]

[a] Department of Mathematics, North Carolina State University, Raleigh, NC 27695-8205, USA
[b] Statistical and Applied Mathematical Sciences Institute, Research Triangle Park, NC 27709-4006, USA

ARTICLE INFO

Article history:
Received 1 September 2011
Received in revised form 27 April 2012
Accepted 28 April 2012
Available online 26 May 2012

Keywords:
Hemodynamics
Network
Transport
Modeling
Boundary conditions
Numerics

ABSTRACT

The structured tree boundary condition is a physiologically-based outflow boundary condition used in hemodynamics. We propose an alternative derivation that is considerably simpler than the original one and yields similar, but not identical, results. We analyze the sensitivity of this boundary condition to its parameters and discuss its domain of validity. Several implementation issues are discussed and tested in the case of arterial flow in the Circle of Willis. Additionally, we compare results obtained from the structured tree boundary condition to the Windkessel boundary condition and measured data.

1. Introduction

The human vascular system is comprised of ten of billions of vessels spanning several orders of magnitude in size. Modeling the entire system with high fidelity approaches from fluid dynamics and elasticity theory is thus not feasible. In many applications, only a specific area of the system is of prime interest. A small number of vessels are then chosen and modeled in detail while the remainder of the vascular network is accounted for through boundary conditions. We focus here on the design, analysis and implementation of conditions at the *outlets* on the boundary of the computational domain, i.e., in those vessels through which blood flows out of the computational domain into the "un-modeled" part of the vasculature.

Significant efforts are currently being devoted to the construction of appropriate boundary conditions for three-dimensional hemodynamics simulations, see for instance [18] or [30]. These issues are fundamental when dealing with a small number of relatively large vessels. For larger networks of smaller vessels, such as in the simulation of cerebral blood flow and perfusion, it has been recently confirmed that there is usually little to be gained by a full three-dimensional computation versus a much simpler one-dimensional approach [6]. The present paper investigates boundary conditions for such one-dimensional formulations.

A variety of boundary conditions have been proposed for one-dimensional models. One option is to prescribe the pressure at each outlet. Although simple to implement, this method has been reported to give physiologically incorrect results in certain cases [7]. Another option involves using an electrical circuit model analogy where pressure and flowrate are respectively

* Corresponding author at: Department of Mathematics, North Carolina State University, Raleigh, NC 27695, USA.
E-mail addresses: wcousin@ncsu.edu (W. Cousins), gremaud@ncsu.edu (P.A. Gremaud).

[1] Partially supported by the National Science Foundation (NSF) through Grant DMS-0636590 and East Asia and Pacific Summer Institutes (EAPSI) award 1015642.
[2] Partially supported by the National Science Foundation (NSF) through Grant DMS-0811150 and through the Statistical and Applied Mathematical Sciences Institute (SAMSI), Grant DMS-0635449.

0021-9991/$ - see front matter © 2012 Elsevier Inc. All rights reserved.
http://dx.doi.org/10.1016/j.jcp.2012.04.038

thought of as voltage and current. Examples of this include a pure resistor model [24], as well as the 3-element RCR Windkessel model [1,3,21,23]. Although each of these methods has been used with success in certain cases (see above references), they have the drawback of not being physiologically based. Additionally, they are sensitive to parameters (resistances and capacitance) which can not be directly measured and must be tuned to generate accurate model output, see for instance [3,10].

The *structured tree boundary condition* or *impedance boundary condition* originates from the work in [28] and was developed by Olufsen [15–17], see also [26]. It remedies some of the undesirable aspects of the above boundary conditions. The vascular trees located downstream from the outlet vessels are assumed to have simple geometric structures – structured trees – subject to certain scaling laws. In addition, a number of drastic simplifying assumptions, including linearization of the governing equations, are made about the fluid dynamics in these trees. This allows for the analytical derivation of a time-dependent expression relating pressure and flowrate at outlets. This boundary condition is physiologically based and can be implemented at moderate computational cost.

The contributions of this paper are as follows. First, we propose in Section 2 a new derivation of the impedance boundary condition. Our approach is much simpler than Olufsen's. The resulting condition is not equivalent but very similar to that of [15–17]. The key difference is that we first average the governing equations on cross-sections and then linearize as opposed to linearizing first and then averaging. Second, we perform, in Section 3, analytical and numerical dependence studies of the impedance boundary condition with respect to its defining geometrical parameters. Model output is found to critically depend on scaling law factors and minimum vessel radius in the tree. Third, Section 4 is devoted to issues related to the numerical implementation of the impedance condition. Its definition as a convolution integral raises both numerical and theoretical questions which are, to the authors' knowledge, discussed here for the first time. We also propose an efficient simplified model allowing for the calculation of the initial flow history. Finally, numerical experiments are discussed in Section 5. Using the example of the Circle of Willis, we compare numerical results obtained with the structured tree boundary condition to numerical results obtained with the Windkessel condition and to data. Conclusions are offered in Section 6.

2. Structured trees

2.1. Geometry of the structured tree

The concept of structured tree in the arterial network, as described for instance in [16], assumes that vessels end by bifurcating into two daughter vessels. Vessels are taken to be cylindrical. For a parent vessel of radius r_p, the radii of the daughter vessels r_{d_1} and r_{d_2} are determined by two scaling parameters ξ and η

$$r_p^\xi = r_{d_1}^\xi + r_{d_2}^\xi,$$
$$\eta = \left(r_{d_2}/r_{d_1}\right)^2,$$

where η is the ratio of the cross-sectional areas of the two daughter vessels. The meaning of ξ is less obvious, although $\xi = 2$ corresponds to conservation of area at the bifurcation. Knowledge of these two parameters allows us to express the radii of the two daughter vessels in terms of the radius of the parent

$$r_{d_1} = \alpha r_p, \quad r_{d_2} = \beta r_p,$$

where $\alpha = \left(1 + \eta^{\xi/2}\right)^{-1/\xi}$ and $\beta = \alpha\sqrt{\eta}$. Additionally, the ratio of a vessel's length to its radius, λ, is assumed to be constant. Vessels with radius less than a specified minimum radius, r_{min}, terminate, i.e., they do not bifurcate.

2.2. Hemodynamics in the tree

In [15], Olufsen describes a process by which one may reduce the Navier–Stokes equations to a form that can be solved analytically. The incompressible Navier–Stokes equations are considered in cylindrical coordinates; further, it is assumed that the effect of gravity is negligible, there is no "swirl," (the angular component of velocity is zero), and the flow is axisymmetric. The equations are linearized, solved exactly, and the longitudinal component of the velocity is integrated to give an equation for the flowrate, Q. Both Q and the pressure P are taken to be periodic in time with known period T (typically T is chosen as the period of inflow data). Assuming also that $\partial_t P$ and $\partial_t Q$ are periodic, continuous, and of bounded variation (to ensure that $\partial_t P$ and $\partial_t Q$ have pointwise convergent Fourier series), the following system of equations may be obtained for $\hat{Q}_k$ and $\hat{P}_k$, the Fourier coefficients of Q and P

$$i\omega_k C\hat{P}_k + \partial_x \hat{Q}_k = 0, \tag{1}$$
$$\widehat{Q}_k + \frac{A_0}{\rho}(1 - F_k)\partial_x \widehat{P}_k = 0, \tag{2}$$

where $F_k = \frac{2J_1(w_k)}{w_k J_0(w_k)}$ with J_1 being the first order Bessel function, $w_k = r_0\sqrt{-i\omega_k\rho/\mu}$, $A_0 = \pi r_0^2, r_0$ is the unstressed vessel radius, ρ is the density of blood, and μ is the dynamic viscosity of blood.[3] While the viscosity μ is assumed constant, the appar-

[3] The above derivation requires the explicit use of multidimensional elasticity for the vessel reactions; the presence of a Bessel function in the above expression is a testimony to that. The derivation proposed below only requires a simple constitutive law, see (10).

ent viscosity depends in fact on vessel radius and hematocrit through the Fahraeus–Lindqvist Effect [4,19,20]. We do not take these effects into account in the present work. Solving the above system yields

$$\widehat{P}_k(0) = \cos\left(\frac{\omega_k}{c_k}L\right)\widehat{P}_k(L) + \frac{i}{Cc_k}\sin\left(\frac{\omega_k}{c_k}L\right)\widehat{Q}_k(L), \tag{3}$$

$$\widehat{Q}_k(0) = iCc_k\sin\left(\frac{\omega_k}{c_k}L\right)\widehat{P}_k(L) + \cos\left(\frac{\omega_k}{c_k}L\right)\widehat{Q}_k(L), \tag{4}$$

where $c_k = \sqrt{(1-F_k)\frac{A_0}{\rho C}}$. Further, $C = \frac{dA}{dP}$ is the compliance, see Section 2.3 for details. The impedance Z is now defined by its Fourier coefficients through $\widehat{Z}_k \triangleq \widehat{P}_k/\widehat{Q}_k$. Letting $x = 0$ and $x = L$ denote the two ends of the vessel under consideration, the impedance at one end of the vessel may be expressed in terms of the impedance at the other end

$$\widehat{Z}_k(0) = \frac{\cos\left(\frac{\omega_k L}{c_k}\right)\widehat{Z}_k(L) + i(c_k C)^{-1}\sin\left(\frac{\omega_k L}{c_k}\right)}{\cos\left(\frac{\omega_k L}{c_k}\right) + ic_k C\sin\left(\frac{\omega_k L}{c_k}\right)\widehat{Z}_k(L)}, \tag{5}$$

$$\hat{Z}_0(0) = \lim_{\omega_k\to 0}\widehat{Z}_k(0) = \widehat{Z}_0(L) + \frac{8\mu\lambda}{\pi r_0^3}. \tag{6}$$

In computing the limit in (6), we consider the variable ω_k in (5) in the continuous sense. At each bifurcation, pressure is assumed to be continuous and mass flux is taken to be conserved, i.e.,

$$\widehat{P}_k^{pa}(L) = \widehat{P}_k^{d_1}(0) = \widehat{P}_k^{d_2}(0),$$
$$\widehat{Q}_k^{pa}(L) = \widehat{Q}_k^{d_1}(0) + \widehat{Q}_k^{d_2}(0).$$

These two assumptions yield the following condition for the impedances at the bifurcation

$$\frac{1}{\widehat{Z}_k^{pa}(L)} = \frac{1}{\widehat{Z}_k^{d_1}(0)} + \frac{1}{\widehat{Z}_k^{d_2}(0)}. \tag{7}$$

The structured tree model is closed by assuming the impedance at the ends ($x = L$) of all terminal vessels to be equal to a specific constant denoted Z_{term}. This value is typically taken to be 0 [16,17]; we take $Z_{term} = 0$ in all analysis in this paper. Given merely the radius of the root vessel, the impedance corresponding to that vessel and the entire vascular tree downstream from it may be calculated for any integer k using the above results. The geometric scaling laws determine the length and radii of all vessels in the tree. The terminal impedance is then imposed at the ends of all terminal vessels, and by repeatedly applying expressions (5) and (7) in succession, a value for the impedance of the root vessel is obtained. An explicit description of this algorithm can be found in [17].

2.3. Alternative formulation

In Section 2.2, the governing equations are first linearized, then averaged on cross sections. Reversing this order allows for a drastically simpler derivation of a similar expression for the impedance since no multidimensional elasticity model has to be considered. As is done in [15], blood flow is assumed to follow the axisymmetric, incompressible Navier–Stokes equations. The effect of gravity is neglected. These equations are then simplified to the point where they may be solved exactly. First, the equations are averaged on-cross sections, leading to the classical one-dimensional formulation [2,3,5,23]

$$\partial_t A + \partial_x Q = 0, \tag{8}$$

$$\partial_t Q + \frac{\gamma+2}{\gamma+1}\partial_x\left(\frac{Q^2}{A}\right) + \frac{A}{\rho}\partial_x P = -2\pi(\gamma+2)\frac{\mu}{\rho}\frac{Q}{A}, \tag{9}$$

where A is the cross-sectional area and Q the flowrate; the density ρ is assumed to be constant, μ is the viscosity. The system is closed by a constitutive law for the pressure P, such as [16]

$$P - P_0 = \frac{4Eh}{3r_0}\left(1 - \sqrt{\frac{A_0}{A}}\right), \tag{10}$$

with $A_0 = \pi r_0^2$ being the cross sectional area of the unstressed vessel and E and h are the Young modulus and thickness of the vessel wall. The parameter γ determines the velocity profile. More precisely, the longitudinal velocity expressed in cylindrical coordinates along the main axis of a vessel, is given by

$$u_x(r,x,t) = \frac{\gamma+2}{\gamma}U(x,t)\left(1 - \left(\frac{r}{R(x,t)}\right)^{\gamma}\right),$$

where $R(x,t)$ is the radius of the vessel ($A = \pi R^2$), and $U = Q/A$ is the cross-sectionally averaged velocity.

In a second step, the system (8) and (9) is linearized in A around the constant value A_0. Further, the system is expressed in terms of P and Q, rather than A and Q through a linearization of the constitutive Eq. (10). This results in

$$C\partial_t P + \partial_x Q = 0,$$
$$\partial_t Q + \frac{A_0}{\rho}\partial_x P = -2\pi(\gamma+2)\frac{\mu}{\rho}\frac{Q}{A_0},$$

where $C = \frac{dA}{dP}$ is the compliance. The third and final step consists in assuming that P and Q are periodic in time, giving the following system for their Fourier coefficients

$$i\omega_k C\widehat{P}_k + \partial_x \widehat{Q}_k = 0, \tag{11}$$
$$(i\omega_k + \delta)\widehat{Q}_k + \frac{A_0}{\rho}\partial_x \widehat{P}_k = 0, \tag{12}$$

where $\delta = 2\frac{\mu(\gamma+2)}{\rho r_0^2}$. Solving the above system yields

$$\widehat{Z}_k(0) = \frac{\cos\left(\frac{\omega_k}{d_k}L\right)\widehat{Z}_k(L) + i(d_k C)^{-1}\sin\left(\frac{\omega_k}{d_k}L\right)}{\cos\left(\frac{\omega_k}{d_k}L\right) + id_k C\sin\left(\frac{\omega_k}{d_k}L\right)\widehat{Z}_k(L)}, \tag{13}$$
$$\widehat{Z}_0(0) = \lim_{\omega_k\to 0}\widehat{Z}_k(0) = \widehat{Z}_0(L) + \frac{2(\gamma+2)\mu\lambda}{\pi r_0^3}, \tag{14}$$

where d_k satisfies $d_k^2 = \frac{\omega_k A_0}{(\omega_k - i\delta)\rho C}$ and $\lambda = L/r_0$.

2.4. Comparison

The expressions for the impedances (13) and (14) and (5) and (6) are similar. In fact, the values of the average impedance $\widehat{Z}_0(0)$ are identical for a Poiseuille flow, i.e., for $\gamma = 2$ in (14). For both models, direct evaluation shows $\widehat{Q}_0(0) = \widehat{Q}_0(L)$, i.e., the temporally averaged flow rate is spatially constant throughout the vessel. Denoting the corresponding value $\overline{Q}$, we observe that both (14) (with $\gamma = 2$) and (6) are simply the Hagen–Poiseuille equation [25]

$$\overline{P}(0) - \overline{P}(L) = \frac{8\mu L\overline{Q}}{\pi r_0^4},$$

where $\overline{P}(x) = \widehat{P}_0(x)$. Fig. 1 displays the root impedance when each of these expressions is implemented in the structured tree algorithm, showing that the use of these two expressions yields very similar results.

3. Dependence on minimum radius

In [15], Olufsen performs numerical sensitivity studies with respect to the minimum radius, r_{min}, and concludes that the structured tree boundary condition is highly sensitive to this parameter. We now provide an analytical explanation of this fact by analyzing the average root impedance, $\widehat{Z}_0^{\text{root}}(0)$. Consider first that instead of terminating according to a minimum radius threshold, the tree terminates after a specific number of generations. An induction argument shows that the average root impedance of this equi-generational tree, with N generations, can be expressed as

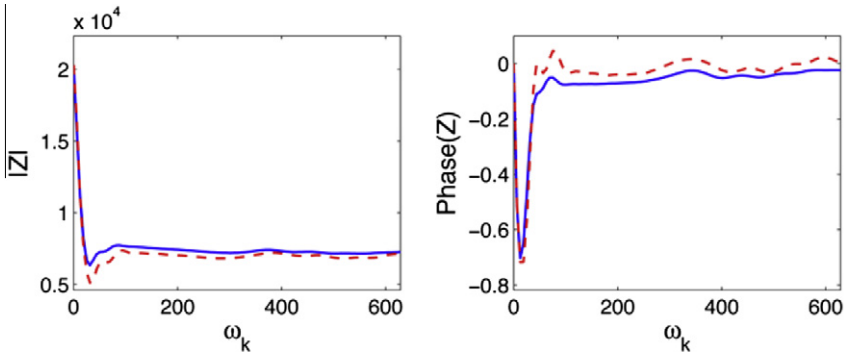

Fig. 1. Modulus and phase of the root impedance generated by the structured tree algorithm using impedance relations (5) (blue, solid curve) and (13) (red, dashed curve). All parameter values (see Table 1) are from [17]. (For interpretation of the references to colour in this figure legend, the reader is referred to the web version of this article.)

Table 1
Parameters used to generate Figs. 1 and 3.

Geometric parameters	$\xi = 2.76,\ \eta = 0.41,\ \lambda = 50,\ r_{\text{root}} = 0.2$ cm, $r_{min} = 70\ \mu$m
Fluid parameters	$\gamma = 2,\ \rho = 1.06$ g cm^{-3}, $\mu = 0.0488$ g cm^{-1} s^{-1}
Elastic relations	$C = 3\pi r^3/2Eh,\ Eh/r = k_1 e^{k_2 r} + k_3$
Elastic parameters	$k_1 = 2.00 \times 10^7$ g s^{-2} cm^{-1}, $k_2 = -22.53$ cm^{-1}
	$k_3 = 8.65 \times 10^5$ g s^{-2} cm^{-1}

$$\widehat{Z}_0^{\text{root}}(0) = \frac{8\mu\lambda}{\pi r_{\text{root}}^3} \sum_{i=0}^{N} \left(\frac{1}{\alpha^3 + \beta^3} \right)^i. \tag{15}$$

We extend this expression to the structured tree with the minimum radius termination criterion via a simple observation: adding an additional generation to a terminal vessel increases the average root impedance. This allows us to use (15) to create upper and lower bounds for the average root impedance

$$\frac{8\mu\lambda}{\pi r_{\text{root}}^3} \sum_{i=0}^{N_1} \left(\frac{1}{\alpha^3 + \beta^3} \right)^i \leqslant \widehat{Z}_0^{\text{root}}(0) \leqslant \frac{8\mu\lambda}{\pi r_{\text{root}}^3} \sum_{i=0}^{N_2} \left(\frac{1}{\alpha^3 + \beta^3} \right)^i, \tag{16}$$

where N_1 and N_2 are the smallest and largest generation terminal vessels, respectively. As $r_{min} \to 0, N_1 \to \infty$. Thus (16) implies that as $r_{min} \to 0, \widehat{Z}_0^{\text{root}}(0)$ behaves like a geometric series which converges only when the quantity $\alpha^3 + \beta^3$ is larger than 1. By definition of the various scaling parameters, we have $\alpha^\xi + \beta^\xi = 1$ and thus

$$\frac{1}{\alpha^3 + \beta^3} < \frac{1}{\alpha^\xi + \beta^\xi} = 1$$

for $\xi > 3$. Therefore, $\hat{Z}_0^{\text{root}}(0)$ converges as $r_{min} \to 0$ if and only if $\xi > 3$.

Physiological and theoretical values of ξ from the literature are given in Table 2. In [13], Murray develops an expression for the work required to operate a section of vessel, and later calculates that a value of $\xi = 3$ minimizes this work [12]. Uylings [29] generalizes Murray's results to include the possibility of non-laminar flow, leading to $\xi = 2.33$ for turbulent flow and agreeing with Murray's $\xi = 3$ in laminar flow. Olufsen proposes $\xi = 2.76$ [16]. Additionally, Suwa et al. [27] and Rossitti and Lofgren [22] have obtained estimated values of ξ by direct measurement. In Table 2, a "sample" refers to a triplet of values (r_p, r_{d1}, r_{d2}) measured at a single bifurcation.

While this collection of measured and theoretically determined values for ξ does exhibit some variation, all of these values share one important characteristic: they are all no bigger than 3. Thus, using *any* of these values will result in the average root impedance being highly sensitive to the choice of r_{min} for small values of r_{min}, since the process is akin to truncating a divergent series.

Fig. 2 shows numerically computed solution curves at a point of the right middle cerebral artery in simulations of the Circle of Willis using values of r_{min} equal to $20, 40, 60, 80$, and $100\ \mu$m. The details of the numerical simulation are given in Section 5. The above analytical result shows that one component of the boundary condition, $\widehat{Z}_0^{\text{root}}(0)$, is sensitive to r_{min}; these numerical results confirm that this sensitivity to r_{min} is also present in the solution itself. For instance, changing r_{min} from 20 μm to 40 μm changes the average pressure at the end of the right middle cerebral artery from 257 mm Hg to 156 mm Hg.

4. Implementation

4.1. Well-definedness of the structured tree boundary condition

The algorithm outlined in Section 2 allows for the calculation of $\widehat{Z}_k = \widehat{P}_k / \widehat{Q}_k$ for each $k \in \mathbb{Z}$ at outlet boundaries of the network. However, implementing these values as a boundary condition is not trivial. In [17], P and Q are described as being related by the following convolution

Table 2
Published values for the scaling parameter ξ.

ξ	Samples	sd	Notes	Source
2.66	1533	0.081	$r \geqslant 100\ \mu$m	Suwa et al. [27]
2.71	1455	0.092	$r < 100\ \mu$m	Suwa et al. [27]
2.9	157	0.7	Measurements from ICA, ACA, MCA	Rossitti and Lofgren [22]
3.0	N/A	N/A	Theoretical optimum, laminar flow	Murray [13]
2.33	N/A	N/A	Theoretical optimum, turbulent flow	Uylings [29]
2.76	N/A	N/A		Olufsen [16]

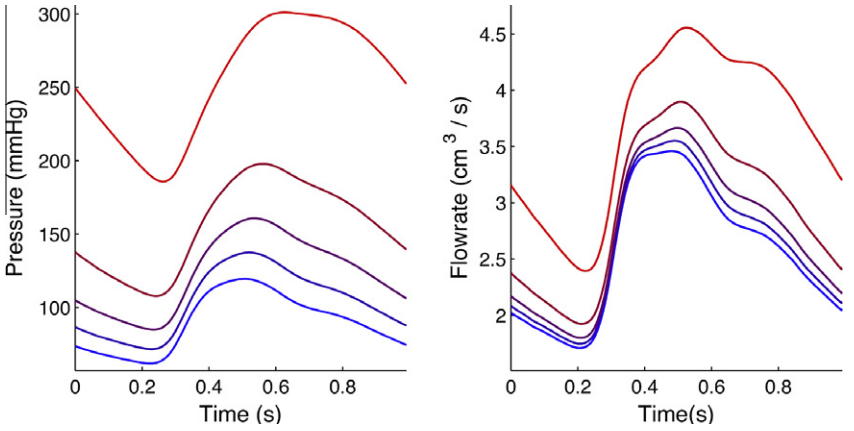

Fig. 2. Pressure and flowrate curves using $r_{min} = 20, 40, 60, 80,$ and100 μm. The red (top) curves correspond to $r_{min} = 20$ μm and the blue (bottom) curves correspond to $r_{min} = 100$ μm. (For interpretation of the references to colour in this figure legend, the reader is referred to the web version of this article.)

$$P(t) = \frac{1}{T}\int_{t-T}^{t} Z(\tau)Q(t-\tau)d\tau, \tag{17}$$

where Z is the function whose Fourier coefficients are $\widehat{Z}_k$. In practice, the integral in (17) is replaced by an N-point quadrature rule ([17] suggests a composite trapezoidal rule), and values of Z are approximated by taking the inverse discrete Fourier transform of N values of $\widehat{Z}_k$. Unfortunately, as suggested by Fig. 1 and proven in the Appendix, $\widehat{Z}_k$ does not converge to 0 as $k \to \infty$ and thus, by the Riemann–Lebesgue Lemma, the integral in (17) does not exist as written.

It is however possible to derive a mathematically sensible boundary condition from the impedance values. Consider the Fourier series expansion for the pressure

$$P(t) = \sum_{k=-\infty}^{\infty} \widehat{P}_k e^{i\omega_k t} = \sum_{k=-\infty}^{\infty} \widehat{Z}_k \widehat{Q}_k e^{i\omega_k t}. \tag{18}$$

In Section 2, $\partial_t Q$ was taken to be continuous and Q periodic. This implies that the Fourier coefficients of Q, $\{\widehat{Q}_k\}$, are in ℓ^1. Additionally, since the sequence $\widehat{Z}_k$ converges to a finite limit, it is bounded. These two facts imply that the expression (18) is well-defined since the series converges absolutely.

The implementation of (18) can only use a finite number of values of Q. A natural choice is to replace the series in (18) by a partial sum and approximate $\widehat{Q}_k$ by computing the discrete Fourier transform of the values of Q. Using an analogue of the Poisson summation formula for Fourier series, as well as the fact that $\{\widehat{Q}_k\} \in \ell^1$, it can be shown that this process is an asymptotically valid approximation to (18) as $N \to \infty$, i.e.

$$\lim_{N\to\infty} \sum_{-\frac{N-1}{2}}^{\frac{N-1}{2}} \widehat{Z}_k \widetilde{Q}_k^{(N)} e^{i\omega_k t} = \sum_{k=-\infty}^{\infty} \widehat{Z}_k \widehat{Q}_k e^{i\omega_k t}, \tag{19}$$

where $\widetilde{Q}_k^{(N)}$ is the approximation of $\widehat{Q}_k$ computed by the DFT. To implement (19) as written in the context of a numerical simulation would require the computation of a DFT at every time step to update the values of $\widetilde{Q}_k^{(N)}$. It is possible to rewrite this expression in the following alternative form

$$\sum_{-\frac{N-1}{2}}^{\frac{N-1}{2}} \widehat{Z}_k \widetilde{Q}_k^{(N)} e^{i\omega_k t} = \frac{\Delta t}{T} \sum_{p=m-N}^{m-1} Q((m-p)\Delta t) Z_N(p\Delta t), \tag{20}$$

where the values of Z_N are obtained by applying the inverse discrete Fourier transform to N values of $\widehat{Z}_k$. This expression is relevant for two reasons. First, to compute the approximation to (18), one does not need to perform a DFT at every time step. Instead, it is only necessary to perform a single inverse DFT at the outset of the simulation to compute the values of Z_N. Second, (20) is precisely the equation obtained when one approximates the convolution integral in (17) by the N-point composite trapezoid rule and approximates Z by computing the inverse DFT of N values of $\widehat{Z}_k$. Therefore, the method of "discretizing the integral" in (17) advocated in [17] leads to a correct result even though its justification is lacking. That interpretation is in fact both incorrect and dangerous. For example, one could derive an expression analogous to (20) by using another quadrature rule; this would result in a different and incorrect boundary condition.

4.2. Convergence to periodic regime

We now numerically investigate the claim that the solution becomes periodic. To do so, we rewrite the solution $\vec{u} = [A, Q]$ "modulo T" into a sequence of grid functions $\vec{u}_k(x_m, t_n) \triangleq \vec{u}(x_m, t_n + kT)$. We also define

$$\Delta_k \vec{u} \triangleq \max_{n=1,\dots N, x_m \in \Omega} ||\vec{u}_k(x_m, t_n) - \vec{u}_{k-1}(x_m, t_n)||_\infty,$$

where N is the number of time steps per period and Ω is the set of all spatial points in the network. The components of $\vec{u}_k - \vec{u}_{k-1}$ are scaled by their temporal averages to make $\Delta_k \vec{u}$ a measure of the relative change in the solution from one period to the next. In the case of the structured tree boundary condition, the issue is complicated by the fact that in addition to providing initial data for all unknowns, one must also prescribe an initial history of the flowrate Q for $t \in [-T, 0]$ at the end of each outlet vessel, see (20). To test the dependence of the solution on the initial history of Q, we solve the problem with 1,000 different sets of initial histories of Q for the outflow vessels of the Circle of Willis. We use constant initial histories of Q equidistributed between 0 cm^3/s and 5 cm^3/s. With each choice of initial history, the solution converged to the same limiting periodic regime to a tolerance of $\Delta_k \vec{u} < 10^{-3}$ in five periods or less. This confirms convergence to a periodic regime and only mild dependence of the choice of initial history.

In some cases, such as for large multidimensional simulations, it is desirable to use better guesses for the initial history in order to shorten the initial transient in the solution [7]. This can be achieved by solving directly for the Fourier coefficients in (11) and (12). These equations can be solved in each of the considered vessels under the same boundary conditions as for the original one-dimensional formulation used above. The dimension of the resulting system is given by the product of the number of vessels by the number of unknowns per vessel (2 here, P and Q) by the number of retained Fourier modes. Further, with the exception of the inflow conditions, the resulting equations are linear. The computational cost linked to this approach is negligible compared to solving (8) and (9) numerically.

This method allows for a remarkably accurate approximation of Q with very few Fourier coefficients. In Fig. 3, Q is approximated with five Fourier coefficients, only three of which are computed since Q is real. Taking this approximate solution for Q as an initial history for the numerical simulation of (8) and (9) yields a sizable acceleration of the convergence of $\Delta_N \vec{u}$. Using the accurate initial history yields values of $\Delta_N \vec{u}$ that are roughly 15 times smaller than the values of $\Delta_N \vec{u}$ when a constant initial history is used for each value of N.

4.3. Computational costs

Once the first N $\widehat{Z}_k$'s, Fourier coefficients of the impedance, have been determined (and a corresponding single inverse DFT has been taken, as explained above in Section 4.1, the application of the boundary condition only requires the calculation of the convolution (20) at each time step for each outflow vessel. The overall corresponding costs therefore scale linearly with the number of time steps and the number of outflow vessels.

The calculation of the impedance itself is greatly simplified by the geometric assumptions made in Section 2.1. The constant ratios defined between parent and daughter vessels (α and β) allow the number of *different* vessel sections to grow quadratically with the number of generations, rather than exponentially as it would for a general tree [16].

5. Numerical experiments

We consider the numerical simulation of blood flow in the Circle of Willis, a ring-like structure of arteries in the human brain, see Fig. 4. Vessel radii and length measurements are taken from [3]. Within individual vessels, we use the system (8)

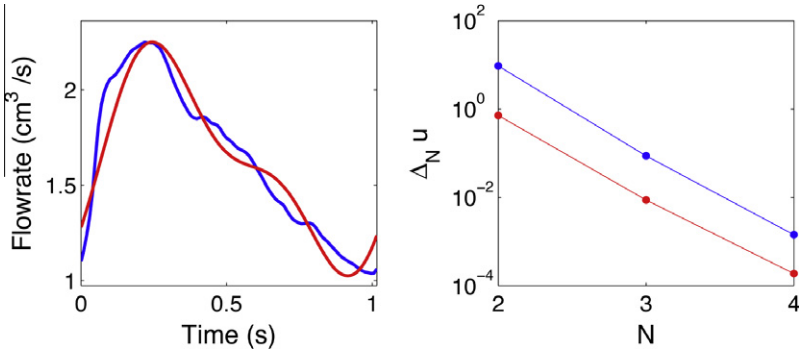

Fig. 3. The left figure denotes the flowrate at the end of the left anterior cerebral artery, obtained by solving (8) and (9) in blue and from approximating five Fourier coefficients in red. On the right, the values of $\Delta_N \vec{u}$ using the approximate solution as an initial history for Q (red) are compared to the same values when using a constant initial history (blue). Parameter values are those from Table 1. (For interpretation of the references to colour in this figure legend, the reader is referred to the web version of this article.)

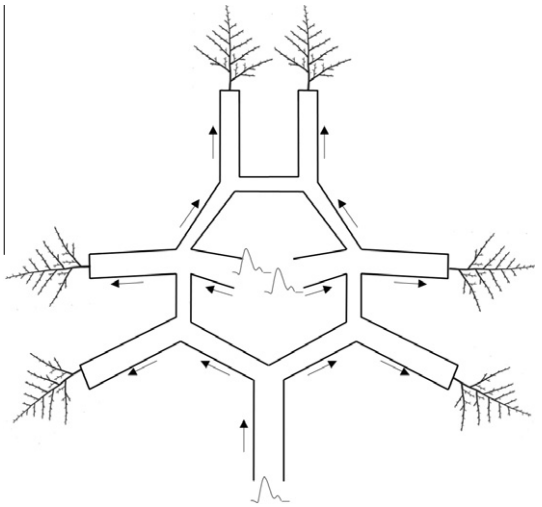

Fig. 4. Schematic representation of the Circle of Willis. Velocity curves indicate inflow vessels, and trees indicate outflow vessels.

and (9) for the cross-sectional area, A, and the flowrate, Q. A characteristic study shows that, at standard operating regime, changes in cross-sectional area and flowrate propagate at speed $U \pm s$, where $U = Q/A$ is the flow velocity and $s > |U|$. In other words, within each vessel, one boundary condition at each end is required.

There are three types of boundaries in this network: inflow/outflow boundaries and junctions. For inflow boundaries, we enforce $\frac{Q}{A} = U$, where U is velocity data measured using digital transcranial Doppler technology at the Beth Israel Deaconess Medical Center. For outflow boundaries, we use the structured tree boundary condition (20). At junctions, we impose mass conservation and continuity of pressure, see [3] for more details and justification. To solve this boundary value problem, we use a Chebyshev collocation method with backward Euler time discretization. All numerical simulations were implemented with a time step of 0.01 s and 6 spatial grid points per vessel. Grid refinement study indicates that this is sufficiently many grid points to ensure reasonable accuracy. This discretization is well adapted to the smooth solutions being sought, has sufficient resolution and is extremely low cost (and is thus well adapted to calibration procedures).

If all inflow boundary conditions used in the above context are periodic of period T, the corresponding solution is expected to become periodic of period T after an initial transient. While the authors are not aware of any corresponding analytical proof, this phenomenon is universally observed in simulation (see below) and is consistent with physiological experience. This periodic long-term solution is of prime interest in perfusion studies.

5.1. Choosing r_{min}: comparison to measured data

As established in Section 3, the value of r_{min} is of critical importance. This issue is exacerbated by the fact that the parameter r_{min} is not strictly physiological, since in the human body arteries do not merely terminate. This rules out the possibility of obtaining r_{min} by direct measurements. However, we show that one may optimize r_{min} to achieve reasonable agreement with measured data. We compare the output of our numerical simulations to velocity measurements at each outflow vessel of the Circle of Willis (Left and Right ACA, MCA, and PCA) as well as blood pressure measurements obtained using a continuous noninvasive finger arterial blood pressure monitor in supine position.[4] The velocity data was obtained using digital transcranial Dopper technology[5] at locations approved by the Institutional Review Board at the Beth Israel Deaconess Medical Center.

We seek to find the 6 values of r_{min} (one each for the Left and Right ACA, MCA, PCA) that minimize the following cost function:

$$\sum_{k=1}^{6} \left\{ \frac{||U^{(k)}_{model} - U^{(k)}_{data}||}{||U^{(k)}_{data}||} + \frac{||P^{(k)}_{model} - P_{data}||}{||P_{data}||} \right\},$$

where $||\cdot||$ denotes the L^2-norm, U denotes velocity, and P denotes pressure. This optimization is complicated by the fact that the model solution is a step function with respect to r_{min} (changing r_{min} either adds vessels, removes vessels, or produces no change). Thus gradient-based optimization methods are unusable, so we implement the Nelder–Mead algorithm, a simplex

[4] Ohmeda, Monitoring Systems, Englewood.
[5] PMD 150, Terumo Cardiovascular Systems and Spencer Technologies Inc, Ann Arbor, MI and Seattle, VA, USA.

Table 3
Optimized values of r_{min} and their corresponding relative errors with respect to measured data.

Vessel	Optimal $r_{min}(\mu m)$	Velocity error	Pressure error
R PCA	109.24	0.126	0.127
R MCA	109.85	0.142	0.128
R ACA	198.37	0.146	0.129
L PCA	83.48	0.066	0.127
L MCA	95.00	0.148	0.128
L ACA	90.03	0.083	0.128

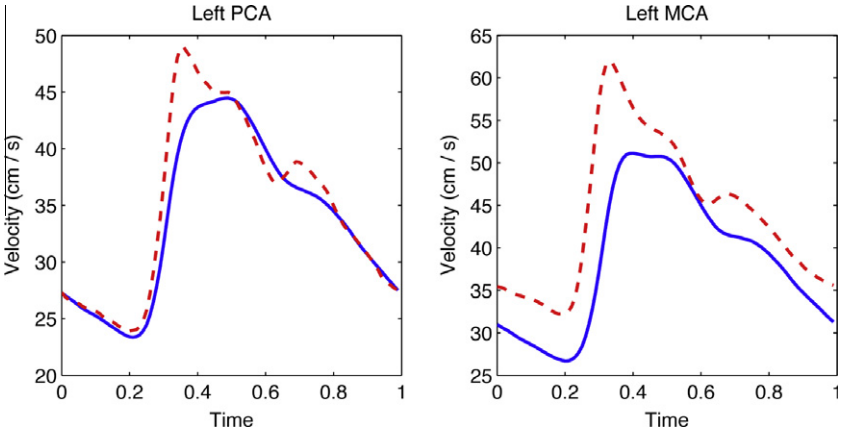

Fig. 5. The blue, solid curve is the model solution, and the red, dashed curve is data. These two vessels were chosen because they represent the best (Left PCA) and worst (Left MCA) fits to data, respectively. (For interpretation of the references to colour in this figure legend, the reader is referred to the web version of this article.)

based direct search method which requires no derivative information [14,9]. We use Tim Kelley's Nelder–Mead MATLAB code [8].

The results in Table 3 and Fig. 5 show that it is possible to choose r_{min} so as to agree reasonably well with data; this is done in a vessel specific fashion. It is worth noticing that we only optimize the minimum radii parameters and that pressure values are measured in the finger.

5.2. Comparison to Windkessel boundary condition

A popular alternative to the structured tree is the 3-element RCR Windkessel boundary condition [1]

$$CR_1R_2\partial_t Q + (R_1 + R_2)Q = CR_2\partial_t P + P. \tag{21}$$

Although the structured tree and Windkessel appear different, we show that remarkably similar results can be obtained by using either boundary condition. If P and Q are periodic with period T and regular enough to be expressed as a uniformly convergent Fourier series, (22) implies the following relation for the values of the impedance

$$\widehat{Z}_k^{WK} = \frac{i\omega_k CR_pR_s + R_p + R_s}{1 + i\omega_k CR_p}, \tag{22}$$

where $\omega_k = 2\pi k/T$. We estimate the parameters C, R_p, and R_s by minimizing the following quantity:

$$\sum_{k=-\frac{N-1}{2}}^{\frac{N-1}{2}} \left|\widehat{Z}_k^{WK} - \widehat{Z}_k^{ST}\right|^2, \tag{23}$$

where $\widehat{Z}_k^{ST}$ denotes the impedance values obtained by the structured tree method using parameters from Table 1. The minimization was done using the Levenberg–Marquardt algorithm [11]. Fig. 6 displays the results in the Anterior Communicating Artery, which is the vessel where these two conditions give results that disagree the *most*. The pressure curves are nearly indistinguishable. The relative L^2 norm of the difference between the two flowrate curves is 6.67×10^{-3}, whereas, in the remainder of the circle of Willis, the two boundary conditions give results differing by no more than 1.42×10^{-4}, roughly 50 times *smaller* than the difference pictured in the flowrate curves in Fig. 6.

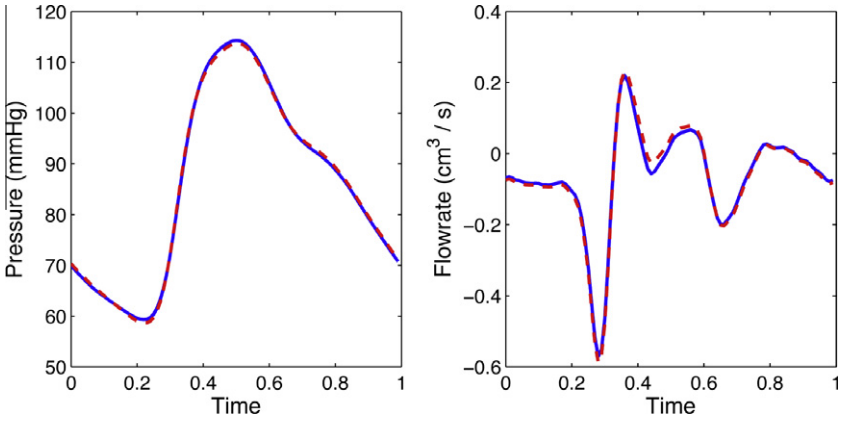

Fig. 6. The blue, solid curve is obtained from the structured tree boundary condition, and the red, dashed curve is the Windkessel. The results pictured are from the Anterior Communicating Artery and the disagreement between the structured tree and the Windkessel is substantially *greater* than the other 15 vessels in the circle of Willis.

6. Conclusion

The structured tree boundary condition has the advantage of being physiologically based, unlike most of the other outflow boundary conditions used in hemodynamics. The analytical and numerical sensitivity studies from Section 3 show the solutions to critically depend on the minimal vessel radius r_{min} which is used in the construction of the impedance. In practice, r_{min} has to be considered as a parameter to be tuned through calibration rather than measured through clinical experimentation. This fact unfortunately mitigates the physiological ties of the method since the retained values of r_{min} have no reason to coincide with, for instance, the radii of the smallest capillaries, as can be shown through implementation.

The derivation of the structured tree model relies heavily on the problem being periodic. This is a reasonable assumption for many clinical studies. There is, however, no justification for using such a model in the study of strokes, sudden vessel occlusion or other abrupt changes in the state of the patient. It would be beneficial if this boundary condition could be extended or reformulated in a way that would allow it to model general transient phenomena. This task is challenging as the periodicity assumption is essential to the reduction of the Navier–Stokes equations, as well as to the use of the discrete values of the impedance as an implementable boundary condition. In the periodic case, our work shows that the results from the Windkessel condition and the structured tree condition can be made nearly identical.

Even if one is primarily interested in the periodic case, the usual approach here is to solve a transient problem with no "built-in periodicity" except possibly in the boundary conditions. The problem is then solved in time until the solution becomes "sufficiently" periodic. This process can be framed as a fixed point iterative process, which requires an initial guess of an entire period of the flowrate at each outlet. Numerical results in Section 4.2 show that it is not necessary to use accurate initial flowrates to achieve convergence, and this limit appears to be independent of this initial guess. However, we show that it is possible to *accelerate* convergence by using an accurate initial guess. We demonstrate a method of computing this accurate initial guess by solving a simplified version of the hemodynamic equations used in the full numerical simulations. It may be possible to extend this method to more complicated cases. For example, one could perform a 1D or 2D simulation to provide an initial guess for the flowrate for a 3D simulation. Doing so could potentially yield substantial computational savings.

Acknowledgments

The authors are indebted to Vera Novak for the use of the cerebral blood velocity data, as well as to Mette Olufsen and Tim David for helpful discussions and insights. They also acknowledge an anonymous referee for remarks that led to a better presentation of the results.

Appendix A. High frequency limit of the impedance

We show that the expression (5) converges to a real, nonzero limit as $\omega_k \to \infty$, which in turn yields the limiting value of the root impedance as $\omega_k \to \infty$. Olufsen [16] evaluates $1 - F_k$ by the use of two different asymptotic expansions (one for $\omega_k \approx 0$, another for large values of ω_k). For large values of ω_k:

$$1 - F_k = 1 - \frac{2}{r}\sqrt{\frac{\mu}{i\omega_k\rho}}.$$

Defining $\overline{C} = L\sqrt{\frac{\rho C}{A_0}},\ \overline{D} = \frac{2}{r}\sqrt{\frac{\mu}{\rho}}$ (note $\overline{C}, \overline{D}$ are positive reals), then

$$\frac{\omega_k L}{c} = \overline{C}\omega_k\left(1 - \overline{D}/\sqrt{i\omega_k}\right)^{-1/2} = \overline{C}\omega_k\left[1 - \overline{D}/\sqrt{2\omega_k} + i\overline{D}/\sqrt{2\omega_k}\right]^{-1/2} = \frac{\overline{C}\omega_k}{\sqrt[4]{1 - \overline{D}\sqrt{\frac{2}{\omega_k}} + \frac{\overline{D}^2}{\omega_k}}} e^{-\frac{i}{2}\arctan(f(\omega_k))},$$

where $f(\omega_k) = \overline{D}/(\sqrt{2\omega_k} - \overline{D})$

$$Im\left(\frac{\omega_k L}{c}\right) = \frac{-\overline{C}\omega_k}{\sqrt[4]{1 - \overline{D}\sqrt{\frac{2}{\omega_k}} + \frac{\overline{D}^2}{\omega_k}}} \sin\left[\frac{1}{2}\arctan\left(f(\omega_k)\right)\right] = \frac{-\overline{C}\omega_k}{\sqrt[4]{1 - \overline{D}\sqrt{\frac{2}{\omega_k}} + \frac{\overline{D}^2}{\omega_k}}} \frac{f(\omega_k)}{\sqrt{\left(1 + \sqrt{1 + f(\omega_k)^2}\right)^2 + f(\omega_k)^2}},$$

since $\lim_{k\to\infty} f(\omega_k) = 0$ and $\lim_{k\to\infty} \omega_k f(\omega_k) = +\infty,\ \lim_{k\to\infty} Im\left(\frac{\omega_k L}{c}\right) = -\infty$ and thus $\lim_{k\to\infty} \tan\left(\frac{\omega_k L}{c}\right) = 1/i$. Notice also that for large $k, Im\left(\frac{\omega_k L}{c}\right) \neq 0$ so $\cos\left(\frac{\omega_k L}{c}\right) \neq 0$ and we may factor out $\cos\left(\frac{\omega_k L}{c}\right)$ from the numerator and denominator of (5) to give:

$$\lim_{k\to\infty} \widehat{Z}_k^{\text{root}}(0) = \lim_{k\to\infty} \frac{\widehat{Z}_k^{\text{root}}(L) + i(cC)^{-1}\tan\left(\frac{\omega_k L}{c}\right)}{1 + icC\tan\left(\frac{\omega_k L}{c}\right)\widehat{Z}_k^{\text{root}}(L)} = \sqrt{\frac{\rho}{A_0 C}}.$$

It is worthy of note that this limit does not depend on any of the root vessel's daughter vessels, and is thus independent of all morphometric parameters (α, β, λ). For example, in Fig. 1, the value of $\lim_{k\to\infty} \hat{Z}_k$ to 2 decimal places is 6970.79.

References

[1] J. Alastruey, K.H. Parker, J. Peiró, S.M. Byrd, S.J. Sherwin, Modeling the circle of willis to assess the effects of anatomical variations and occlusions on cerebral flows, J. Biomech. 40 (2007) 1794–1805.
[2] S. Čanić, E.H. Kim, Mathematical analysis of the quasilinear effects in a hyperbolic model blood flow through compliant axi-symmetric vessels, Math. Methods Appl. Sci. 26 (14) (2003) 1161–1186.
[3] K. DeVault, P.A. Gremaud, V. Novak, M.S. Olufsen, G. Vernieres, P. Zhao, Blood flow in the circle of willis: modeling and calibration, Multiscale Model. Simul. SIAM Interdiscip. J. (2008) 888–909.
[4] R. Fahraeus, T. Lindqvist, The viscosity of blood in narrow capillary tubes, Am. J. Physiol. – Legacy Content 96 (3) (1931) 562–568.
[5] M.A. Fernández, V. Milišić, A. Quarteroni, Analysis of a geometrical multiscale blood flow model based on the coupling of ODEs and hyperbolic PDEs, Multiscale Model. Simul. 4 (1) (2005) 215–236 (electronic).
[6] L. Grinberg, T. Anor, E. Cheever, J.R. Madsen, G.E. Karniadakis, Simulation of the human intracranial arterial tree, Phil. Trans. R. Soc. 367 (2009) 2371–2386.
[7] L. Grinberg, G.E. Karniadakis, Outflow boundary conditions for arterial networks with multiple outlets, Ann. Biomed. Eng. 36 (9) (2008) 1496–1514.
[8] C.T. Kelley, Nelder-mead optimizer [matlab program], 1996. www4.ncsu.edu/ctk/darts/nelder.m.
[9] C.T. Kelley, Iterative Methods for Optimization, SIAM, 1999.
[10] T. Kind, T.J.C. Faes, J.-W. Lankhaar, A. Vonk-Noordegraaf, M. Verhaegen, Estimation of three- and four-element windkessel parameters using subspace model identification, IEEE Trans. Biomed. Eng. 57 (2010) 1531–1538.
[11] Donald W. Marquardt, An algorithm for least-squares estimation of nonlinear parameters, SIAM J. Appl. Math. 11 (1963) 431–441.
[12] C.D. Murray, The physiological principle of minimum work applied to the angle of branching of arteries, J. Gen. Physiol. 9 (6) (1926) 835–841.
[13] C.D. Murray, The physiological principle of minimum work I: the vascular system and the cost of blood volume, Proc. Nat. Acad. Sci. USA 12 (3) (1926) 207–214.
[14] J.A. Nelder, R. Mead, A simplex method for function minimization, Comput. J. 7 (4) (1965) 308–313.
[15] M.S. Olufsen, Modeling the arterial system with reference to an anesthesia simulator, PhD. thesis, Roskilde University, Denmark, 1998, pp. 95–120.
[16] M.S. Olufsen, Structured tree outflow condition for blood in the larger systemic arteries, Am. J. Physiol. 276 (Heart Circ. Physiol. 45) (1999) H257–H268.
[17] M.S. Olufsen, C.S. Peskin, W.Y. Kim, E.M. Pederson, A. Nadim, J. Larsen, Numerical simulation and experimental validation of blood flow in arteries with structured-tree outflow conditions, Ann. Biomed. Eng. 28 (2000) 1281–1299.
[18] N.M. Pahlevan, F. Amlani, M. Hossein Gorji, F. Hussain, M. Gharib, A physiologically relevant, simple outflow boundary model for truncated vasculature, Ann. Biomed. Eng. 39 (2011) 1470–1481.
[19] A.R. Pries, D. Neuhaus, P. Gaehtgens, Blood viscosity in tube flow: dependence on diamter and hematocrit, Am. J. Physiol. 263 (Heart Circ. Physiol. 32) (1992) H1770–H1778.
[20] A.R. Pries, T.W. Secomb, T Gessner, M.B. Sperandio, J.F. Gross, P. Gaehtgens, Resistance to blood flow in microvessels in vivo, Circ. Res. 75 (1994) 904–915.
[21] A. Quarteroni, M. Tuveri, A. Veneziani, Computational vascular fluid dynamics: problems, models and methods, Comput. Visual. Sci. 2 (2000) 163–197.
[22] S. Rossitti, J. Lofgren, Vascular dimensions of the cerebral arteries follow the principle of minimum work, Stroke 34 (1992) 371–377.
[23] S.J. Sherwin, V. Franke, J. Peiró, K. Parker, One-dimensional modelling of a vascular network in space-time variables, J. Engrg. Math. 47 (3–4) (2003) 217–250.
[24] S.J. Sherwin, L. Formaggia, J. Peiró, V. Franke, Computational modeling of 1d blood flow with variable mechanical properties and its application to simulation of wave propagation in the human arterial system, Int. J. Num. Methods Fluids 43 (2003) 673–700.
[25] J.H. Spurk, Fluid Mechanics, Springer, Berlin, 1997.
[26] B.N. Steele, C.A. Taylor, Simulation of blood flow in the abdominal aorta at rest and during exercise using a 1-d finite element method with impedance boundary conditions derived from a fractal tree, in: Proc. 2003 ASME Summer Bioeng. Meeting, Key Biscayne, FL, 2003.
[27] N. Suwa, T. Niwa, H. Fukasawa, Y. Sasaki, Estimation of intravascular blood pressure gradient by mathematical analysis of arterial casts, Tohoku J. Exp. Med. 79 (1963) 168–198.
[28] M.G. Taylor, Wave transmission through an assembly of randomly branching elastic tubes, Biophys. J. 6 (1966) 697–716.
[29] H.B.M. Uylings, Optimization of diameters and bifurcation angles in lung and vascular tree structures, Bull. Math. Biol. 39 (1977).
[30] I.E. Vignon-Clementel, C.A. Figueroa, K.E. Jansen, C.A. Taylor, Outflow boundary conditions for 3d simulations of non-periodic blood flow and pressure fields in deformable arteries, Comput. Methods Biomech. (2010) 1–16.